# Analysis of Mixed-Mode Fracture in Concrete

By Jan G. Rots[1] and René de Borst[2]

**Abstract:** A smeared crack model that covers tensile softening in mode I and shear softening in mode II fracture is described. In addition, the model provides for unloading and reloading and for multiple crack formation. Particular forms of tension and shear softening functions and relations with more conventional models are discussed. Two examples involving mixed-mode fracture in notched, unreinforced concrete beams have been included to demonstrate the versatility of the model. The results indicate that the addition of shear softening is essential to obtain realistic results in the post-peak regime since the classical approach based on a constant shear retention factor then results in a too stiff behavior. The results furthermore demonstrate that snap-back behavior may occur in strain-softening concrete under quasistatic loading conditions. Attention is also given to the possibility of hour-glass formation when constitutive laws involving softening are deployed in a finite element model.

## Introduction

The development of powerful finite element codes for analyzing concrete structures has very much stimulated the interest in constitutive laws for concrete. At present, a considerable number of models are available for the behavior of concrete under compressive stresses, for the long-term behavior of concrete, for simulating crack initiation and propagation, etc. With regard to the latter, Hillerborg et al. (1976) and Bažant and Oh (1983) have developed sophisticated tensile softening formulations to simulate the mode I cracking behavior of concrete, which have subsequently been implemented in a number of finite element codes (e.g., Crisfield 1986; Glemberg 1984; Ingraffea and Gerstle 1985; Leibengood et al. 1986; Rots et al. 1984, 1985; William and Sture 1985).

Less attention has been paid to the modeling of shear transfer across a crack. Indeed, some formulations exist for modeling crack dilatancy (e.g., Bažant and Gambarova 1980; Reinhardt and Walraven 1982), but almost all numerical applications deploy a so-called shear retention factor $\beta$ (Suidan and Schnobrich 1973) to model aggregate interlock. This is a rather coarse method, especially when we consider that $\beta$ is usually assigned a constant value, so that there is a linear ascending relation between shear stress increment and shear strain increment across the crack. Some researchers have considered the assumption of a constant shear retention factor too crude (e.g., Cedolin and Dei Poli 1977; Kolmar and Mehlhorn 1984) and have made it a descending function of the crack normal strain, assigning it

[1]Res. Engr., Delft Univ. of Tech., Dept. of Civ. Engrg., P.O. Box 5048, 2600 GA Delft, Netherlands.

[2]Res. Engr., TNO Inst. for Building Materials and Struct., Software Engrg. Dept., P.O. Box 49, 2600 AA Delft, Netherlands.

Note. Discussion open until April 1, 1988. To extend the closing date one month, a written request must be filed with the ASCE Manager of Journals. The manuscript for this paper was submitted for review and possible publication on December 15, 1986. This paper is part of the *Journal of Engineering Mechanics*, Vol. 113, No. 11, November, 1987. ©ASCE, ISSN 0733-9399/87/0011-1739/$01.00. Paper No. 21979.

a zero or almost zero value for large crack strains. But even with this improvement, we still face the anomaly that for large crack strains a large, constant shear stress is being transmitted across the crack. To remedy this, a shear softening relation will be used herein for mode II crack propagation.

The discrepancy between the sophisticated constitutive models developed for cracks and the coarse models used in finite element analysis, especially when the smeared crack approach is adopted, is partly due to the specific smeared crack model deployed in most finite element codes. Recently, de Borst and Nauta (1984,1985) and Rots et al. (1985) have proposed a smeared crack formulation which obviates a number of objections that adhere to the standard smeared crack approach. This model, which provides for multidirectional cracking owing to rotation of the principal stress axes after primary crack formation and which is independent of the constitutive model for the intact concrete between the cracks, is also well-suited for the implementation of sophisticated softening relations, both in tension (mode I) and in shear (mode II). For this reason the paper starts with a review of the crack model and softening relations used. Next, two mixed-mode fracture analyses displaying tensile and shear softening will be presented, along with a discussion about the existence of shear fracture.

Two other aspects to which we will draw attention is snap-back behavior, which may occur in concrete structures, and the danger of hour-glassing when softening-type constitutive laws are deployed in a finite element model. It has been demonstrated that such phenomena may easily occur when a tensile softening relation is employed (de Borst and Nauta 1985; de Borst 1986; Crisfield 1986; Rots 1985b). We will indicate that the difficulties are even greater in the presence of shear softening.

## Smeared Crack Model

The fundamental feature of the smeared crack model employed is a decomposition of the total strain increment into a concrete strain increment $\Delta\boldsymbol{\varepsilon}^{co}$ and a crack strain increment $\Delta\boldsymbol{\varepsilon}^{cr}$:

$$\Delta\boldsymbol{\varepsilon} = \Delta\boldsymbol{\varepsilon}^{co} + \Delta\boldsymbol{\varepsilon}^{cr} \quad \ldots\ldots (1)$$

As pointed out by Litton (1974) and de Borst and Nauta (1984,1985) the crack strain increment $\Delta\boldsymbol{\varepsilon}^{cr}$ may also be composed of several contributions:

$$\Delta\boldsymbol{\varepsilon}^{cr} = \Delta\boldsymbol{\varepsilon}_1^{cr} + \Delta\boldsymbol{\varepsilon}_2^{cr} + \ldots\ldots (2)$$

in which $\Delta\boldsymbol{\varepsilon}_1^{cr}$ = strain increment owing to a primary crack; $\Delta\boldsymbol{\varepsilon}_2^{cr}$ = strain increment owing to a secondary crack, and so on.

The relation between the crack strain increment of a particular crack (either primary or secondary) and the stress increment is conveniently defined in the coordinate system, which is aligned with the crack. This necessitates a transformation between the crack strain increment $\Delta\boldsymbol{\varepsilon}_n^{cr}$ of crack $n$ in the global $x$, $y$ and $z$ coordinates and a crack strain increment $\Delta\boldsymbol{\varepsilon}_n^{cr}$, which is expressed in local coordinates. Restricting the treatment to a two-dimensional configuration (which is not essential), we observe that a

crack only has a normal strain increment $\Delta e_n^{cr}$ (mode I) and a shear strain increment $\Delta\gamma_n^{cr}$ (mode II), so that

$$\Delta\mathbf{e}_n^{cr} = (\Delta e_n^{cr}\ \Delta\gamma_n^{cr})^T \quad \ldots\ldots (3)$$

in which the superscript $T$ denotes a transpose. The relation between $\Delta\boldsymbol{\varepsilon}_n^{cr}$ and $\Delta\mathbf{e}_n^{cr}$ reads

$$\Delta\boldsymbol{\varepsilon}_n^{cr} = \mathbf{N}_n \Delta\mathbf{e}_n^{cr} \quad \ldots\ldots (4)$$

$$\text{with}\quad \mathbf{N}_n = \begin{bmatrix} \cos^2\vartheta_n & -\sin\vartheta_n & \cos\vartheta_n \\ \sin^2\vartheta_n & \sin\vartheta_n & \cos\vartheta_n \\ 2\sin\vartheta_n\cos\vartheta_n & \cos^2\vartheta_n & -\sin^2\vartheta_n \end{bmatrix} \quad \ldots\ldots (5)$$

in which $\vartheta_n$ = inclination angle of the normal of crack $n$ with the $x$ axis.

Substitution of Eq. 5 into Eq. 2 gives for multiple cracks

$$\Delta\boldsymbol{\varepsilon}^{cr} = \mathbf{N}_1\Delta\mathbf{e}_1^{cr} + \mathbf{N}_2\Delta\mathbf{e}_2^{cr} + \ldots\ldots (6)$$

For the derivation of the stress-strain law of the system of cracks and concrete, it is convenient to assemble all the crack strain increments, which are expressed in their own local coordinate system in a vector $\Delta\mathbf{e}^{cr}$

$$\Delta\mathbf{e}^{cr} = (\Delta e_1^{cr}\ \Delta\gamma_1^{cr}\ \Delta e_2^{cr}\ \Delta\gamma_2^{cr}\ \ldots)^T \quad \ldots\ldots (7)$$

Introducing the matrix $\mathbf{N}$,

$$\mathbf{N} = [\mathbf{N}_1\mathbf{N}_2\ \ldots] \quad \ldots\ldots (8)$$

we observe that we can rewrite Eq. 7 as

$$\Delta\boldsymbol{\varepsilon}^{cr} = \mathbf{N}\Delta\mathbf{e}^{cr} \quad \ldots\ldots (9)$$

In a similar way, we can define a vector $\Delta\mathbf{s}_n$

$$\Delta\mathbf{s}_n = (\Delta s_1\ \Delta t_1)^T \quad \ldots\ldots (10)$$

with $\Delta s_n$ the normal and $\Delta t_n$ the shear stress increment in crack $n$ of the integration point. The vector $\Delta\mathbf{s}$, which assembles all the stress increments with respect to their own local coordinate system, then reads:

$$\Delta\mathbf{s} = (\Delta s_1\ \Delta t_1\ \Delta s_2\ \Delta t_2\ \ldots)^T \quad \ldots\ldots (11)$$

The relation between the stress increment in the global coordinate system $\Delta\boldsymbol{\sigma}$ and the stress vector $\Delta\mathbf{s}$ can subsequently be derived to be

$$\Delta\mathbf{s} = \mathbf{N}^T\Delta\boldsymbol{\sigma} \quad \ldots\ldots (12)$$

To complete the system of equations, we need a constitutive model for the intact concrete and a stress-strain relation for the smeared cracks. For the concrete between the cracks we assume a relationship of the following structure

$$\Delta\boldsymbol{\sigma} = \mathbf{D}^{co}\ \Delta\boldsymbol{\varepsilon}^{co} \quad \ldots\ldots (13)$$

with the matrix $\mathbf{D}^{co}$ containing the instantaneous moduli of the concrete. As attention is focused on the behavior of concrete under tensile stresses, $\mathbf{D}^{co}$ has simply been assumed to be the elasticity matrix, but analyses have

already been performed with elastoplastic (de Borst and Nauta 1985) and visco-elastic (de Borst and van den Berg 1986) concrete properties.

In a similar way, we can define a relation between the crack strain increment $\Delta \mathbf{e}_n^{cr}$ of crack $n$ and the stress increment $\Delta \mathbf{s}_n$ in that crack. In this paper a relation is assumed, which formally reads:

$$\Delta \mathbf{s}_n = \mathbf{D}_n^{cr} \, \Delta \mathbf{e}_n^{cr} \quad \ldots\ldots (14)$$

with $\mathbf{D}_n^{cr}$ a 2*2 matrix. For the derivation of the stress-strain relation of the cracked concrete, it is again convenient to assemble all the matrices $\mathbf{D}_n^{cr}$ in one matrix $\mathbf{D}^{cr}$, which is defined as

$$\mathbf{D}^{cr} = \begin{bmatrix} \mathbf{D}_1^{cr} & \mathbf{0} & \cdots \\ \mathbf{0} & \mathbf{D}_2^{cr} & \cdots \\ \cdots & \cdots & \cdots \end{bmatrix} \quad \ldots\ldots (15)$$

so that the relation between $\Delta \mathbf{s}$ and $\Delta \mathbf{e}^{cr}$ reads

$$\Delta \mathbf{s} = \mathbf{D}^{cr} \, \Delta \mathbf{e}^{cr} \quad \ldots\ldots (16)$$

Using Eqs. 1, 9, 12, 13 and 16 we can develop the stress-strain relation for the cracked concrete:

$$\Delta \boldsymbol{\sigma} = [\mathbf{D}^{co} - \mathbf{D}^{co}\mathbf{N}(\mathbf{D}^{cr} + \mathbf{N}^T\mathbf{D}^{co}\mathbf{N})^{-1}\mathbf{N}^T\mathbf{D}^{co}]\Delta \boldsymbol{\varepsilon} \quad \ldots\ldots (17)$$

Independently, a similar framework for a smeared crack model was recently developed by Riggs and Powell (1986), following the original ideas of Litton (1974).

## Mode I Tensile Softening and Mode II Shear Softening

In the previous sub-section, Eq. 14, which relates the crack strain increment $\Delta \mathbf{e}_n^{cr}$ and the stress increment $\Delta \mathbf{s}_n$, was introduced without specifying the crack constitutive matrix $\mathbf{D}_n^{cr}$. The framework of the model permits $\mathbf{D}_n^{cr}$ to be nonsymmetric, which for instance occurs in dilatancy theories for sliding along preexisting macrocracks (e.g., Bažant and Gambarova 1980; Reinhardt and Walraven 1982). However, in this paper attention is focused on fracture initiation and propagation rather than on sliding along existing fracture planes. In such cases the crack strains are relatively small and the off-diagonal terms in $\mathbf{D}_n^{cr}$ are expected to be less important. Consequently, the off-diagonal terms have been set equal to zero in the sample problems to be shown, so that $\mathbf{D}_n^{cr}$ reduces to:

$$\mathbf{D}_n^{cr} = \begin{bmatrix} D^I & 0 \\ 0 & D^{II} \end{bmatrix} \quad \ldots\ldots (18)$$

in which $D^I$ = mode I tensile softening modulus and $D^{II}$ = mode II shear softening modulus.

Considering the tensile softening modulus $D^I$ first, we observe that this modulus may be related to three basic tensile softening parameters, viz., the direct tensile strength $f_{ct}$, the fracture energy $G_f^I$ (defined as the amount of energy required to create one unit of area of a mode I crack) and the shape of the tensile softening diagram. In this paper the tensile softening diagram proposed by Cornelissen et al. (1986) has been adopted (Fig. 1).

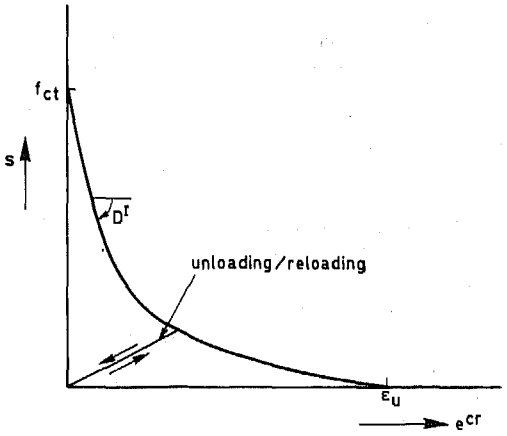


**FIG. 1. Mode I Tensile Softening Relation between Normal Stress and Crack Normal Strain**

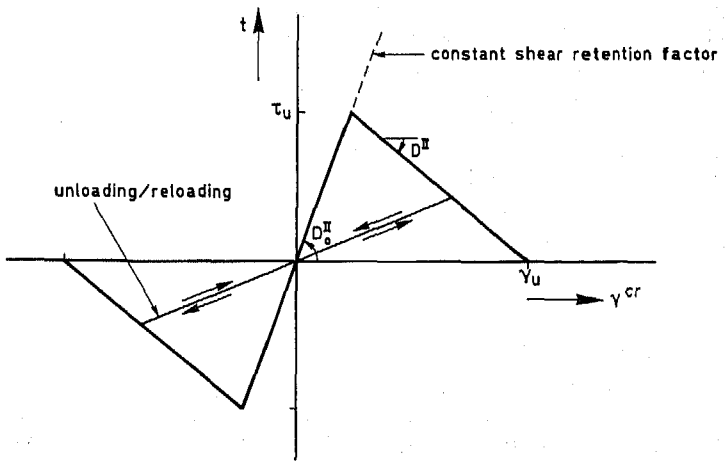


**FIG. 2. Mode II Shear Softening Relation between Shear Stress and Crack Shear Strain**

A shear softening formulation is less common than a tensile softening formulation, but can be set up along similar lines. The shear softening modulus $D^{II}$ in Eq. 18 might also be related to three parameters, viz., an ultimate shear stress $\tau_u$ transferred across the crack, a fracture energy $G_f^{II}$ (defined as the amount of energy required to create one unit of area of a pure mode II crack) and a specific shape of the shear softening diagram. Here applications are restricted to a bilinear shape of the shear softening diagram, in particular to a diagram linearly ascending to the ultimate stress $\tau_u$, followed by a linear descending branch, as shown in Fig. 2.

The present formulation assumes fracture to be initiated normal to the

axis of the principal tensile stress. A direct consequence of this crack initiation criterion is that the shear stress across the crack is zero at the onset of cracking, which explains why the shear softening diagram of Fig. 2 starts in the origin. Only upon subsequent rotation of the principal stress axes a shear stress may develop across the crack faces until its maximum level $\tau_u$ whereafter the shear softening branch is entered.

The fracture energy values are assumed to be fixed material properties. In mode I this postulate seems to be justified because experimental data show that the energy required to fracture mode I specimens is fairly proportional to the surface area generated. However, in mode II fracture this question is far from resolved. Nevertheless, we have adopted the assumption that the fracture energy released in mode II fracture is also a material property because it is simple and more realistic than a constant shear retention factor, which in fact prohibits energy from being dissipated in mode II fracture.

In a smeared crack environment fracture is usually assumed to be distributed over a certain crack band width $h$, which is related to the particular finite element configuration. Consequently, the fracture energy should be released over this width to obtain finite element results that are objective with regard to mesh refinement. With respect to the mode I fracture energy this has been achieved by adjusting the tensile softening modulus $D^I$ and the stress-free crack normal strain $\varepsilon_u$ (see Fig. 1) to $h$, following the crack band theory of Bažant and Oh (1983). A similar procedure has been adopted to control mesh-objective release of the mode II fracture energy. Assuming a constant shear strain distribution over the crack band, the mode II fracture energy is represented by the integral of the shear softening diagram multiplied by the crack band width. For the triangular shear softening diagram of Fig. 2 this results in a stress-free crack shear strain $\gamma_u$ equal to

$$\gamma_u = \frac{2G_f^{II}}{\tau_u h} \qquad (19)$$

## Unloading, Closing and Reopening Cracks

Fracture localization involves simultaneous unloading of adjacent elements and localization can only be captured accurately if the model includes provisions for unloading in addition to softening. Indeed, smeared crack analyses are known to exhibit quite a number of cracks that unload, even close and sometimes reopen again in a later stage of the loading process (de Borst and Nauta 1985; Crisfield 1986; Leibengood et al. 1986; Rots et al. 1985).

In this study unloading and reloading phenomena have been modeled using a secant approach, which implies that upon unloading the stress follows a straight line back to the origin. This procedure has been adopted both for mode I and for mode II fracture, as indicated in Figs. 1 and 2. Again, any coupling between mode I and mode II behavior has been ignored, so that it is possible for a crack to soften in mode I and unload in mode II, to unload in mode I and soften in mode II, to soften in both modes, or to unload in both modes.

Complete closing of a crack has been assumed when both the crack normal stress and the crack normal strain vanish. This, however, need not

be true for the crack shear stress and the crack shear strain; therefore, these quantities are stored upon closing. Once closed, the crack is subjected to compression and the elastic behavior is recovered.

A closed crack is permitted to reopen when the stress normal to the crack again becomes tensile. In the tensile softening diagram the crack then follows the secant branch until the residual tensile strength, whereafter the softening branch is entered. The behavior in mode II upon reopening is a different issue. It is likely that the principal stresses will rotate while the crack is closed, so that the crack shear stress that exists upon reopening differs significantly from the crack shear stress that existed upon closing. The following procedure, which appeared to be numerically stable, has been adopted. The starting point in the shear softening diagram was assumed to be given by the crack shear stress upon reopening and the crack shear strain which was stored upon closing. Because of the stress rotations during the closed state this crack shear stress/crack shear strain combination will not be positioned on the prescribed shear softening diagram of Fig. 2. For this reason, the crack was assumed to soften in mode II immediately upon reopening, following a different shear softening diagram than the one prescribed but consuming the same amount of mode II fracture energy. The peak of this adapted shear softening diagram was assumed to correspond with the crack shear stress/crack shear strain combination upon reopening and the stress-free strain of the diagram was assumed to be given by Eq. 19 with the crack shear stress upon reopening substituted instead of the prescribed ultimate stress $\tau_u$.

## Relation with Other Crack Shear Formulations

Within smeared crack models not based upon a decomposition of the total strain increment into concrete and crack strain increment it has become accepted practice to represent the shear stiffness of cracked concrete by means of a shear retention factor $\beta$, indicating the percentage of the initial elastic shear capacity retained after cracking. Hence, the elastic shear modulus $G$ is reduced to $\beta G$ once the material has cracked ($\beta \leq 1$).

The shear retention factor $\beta$ can be related to the crack shear modulus $D^{II}$ of the present model by considering that the stiffness $\beta G$ is associated with the total strain increment, whereas the crack shear modulus $D^{II}$ is associated solely with the crack strain increment. Furthermore, the strain decomposition of Eq. 1 implies that the present model assumes concrete and crack to be connected in series, so that the following stiffness relation holds:

$$\frac{1}{\beta G} = \frac{1}{G} + \frac{1}{D^{II}} \qquad (20)$$

Consequently, the initial modulus $D_0^{II}$ of the shear softening diagram of Fig. 2 can alternatively be expressed by an initial shear retention factor $\beta_0$:

$$\beta_0 = \frac{D_0^{II}}{D_0^{II} + G} \qquad (21)$$

The shear softening formulation further bears some similarities to the frictional slip model proposed by Willam and Sture (1985). Their model is

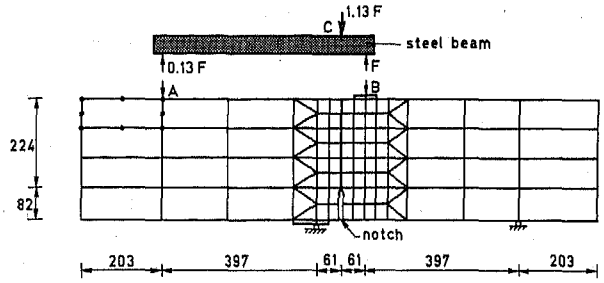


**FIG. 3. Finite Element Idealization for Single-Notched Specimen**

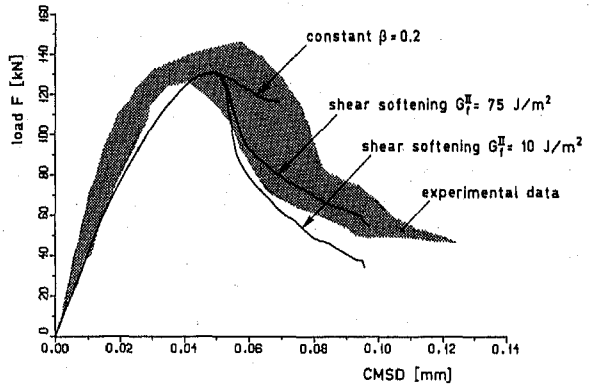


**FIG. 4. Load versus CMSD Computed for Three Different Crack Shear Representations (Shaded Area Denote Range of Experimental Results)**

primarily meant to simulate shear band formation in multiaxial compression, whereas the present model is directed toward mixed-mode fracture occurring in the tension-tension and tension-compression quadrants of the principal stress space. This emerges from the fact that Willam and Sture (1985) assume the softening to start in mode II, while the present model assumes the softening to start in mode I and only considers the mode II effects because of subsequent rotation of stresses. In the former case the shear stress upon fracture initiation reaches a maximum rather than being zero, and the value of the mode II fracture energy may be higher.

## Single-Notched Specimen

The first example concerns an unreinforced single-notched beam which has been tested by Arrea and Ingraffea (1982). Fig. 3 shows the finite element idealization. The beam has been analyzed using eight-noded plane stress elements, which have been integrated using nine-point Gaussian quadrature. In the transition region between the coarse part and the fine part of the mesh, three-point integrated six-noded triangles were used. The beam had a thickness of 156 mm. Fig. 3 indicates that the loading

conditions are nonsymmetric, which implies that the fracture propagating from the notch will show opening as well as sliding (mixed-mode). Consequently, both tensile softening and shear softening are of interest.

In the experiment the load was applied at point C of the steel beam AB and was controlled by a feedback mechanism with the Crack Mouth Sliding Displacement (CMSD) as a control parameter. A numerical analogy thereof is the "indirect displacement control" scheme recently developed by de Borst (1986). Indirect displacement control differs from the standard arc-length control schemes (Crisfield 1981; Ramm 1981; Riks 1979) in that it involves a constraint equation based on a few dominant displacement parameters rather than on a global norm of displacement increments. This technique has proved to be essential for stabilizing the post-peak regime in case of strong localizations that occur in crack propagation. Consequently, the analyses have been performed under indirect displacement control, with the CMSD being the control parameter.

The concrete has been modeled as linearly elastic in compression with a Young's modulus $E_c = 24{,}800$ N/mm$^2$ and a Poisson ratio $\nu = 0.18$. This approach is justified because the compressive stresses remain low enough to avoid nonlinearity in compression. The mode I crack parameters have been assigned the following values: tensile strength $f_{ct} = 2.8$ N/mm$^2$, mode I fracture energy $G_f^I = 75$ J/m$^2$ and intercrack threshold-angle $\alpha = 60°$ (de Borst and Nauta 1985). The crack band width has been estimated as $h = 20.3$ mm.

Three analyses have been performed. First, a constant shear retention factor $\beta_0 = 0.2$ has been adopted, which corresponds to a linear ascending branch in the crack shear diagram with a stiffness modulus $D_0^{II} = 2{,}627$ N/mm$^2$ (compare Eq. 21). In the other two analyses the same initial shear retention factor has been employed, but shear softening has been added in the form of the triangular shear softening diagram of Fig. 2. The mode-II fracture energy values for these two analyses have been assumed to be $G_f^{II} = 75$ J/m$^2$ and $G_f^{II} = 10$ J/m$^2$, respectively, whereas in both cases the ultimate crack shear stress was $\tau_u = 0.5$ N/mm$^2$.

Fig. 4 shows that the computational result for the load-CMSD response nicely falls within the experimental scatter when shear-softening is added, whereas a deviation occurs in the post-peak regime when a constant shear retention factor is employed. The analysis with the constant shear retention factor yields about the same limit load, but shows far too little softening in the post-peak regime, which is entirely due to the fact that the shear stress across the cracks is allowed to increase indefinitely. For some integration points we even observed a crack shear stress amounting to 15 N/mm$^2$, which is unrealistic, since any confinement in the form of compression normal to the crack was lacking. The addition of local shear softening clearly turns out to be essential for producing global softening for structures that fail in mixed-mode fracture.

In addition to the load-CMSD response, the load-CMOD response has been recorded, as shown in Fig. 5 (CMOD = Crack Mouth Opening Displacement). Initially, the CMOD is negative, but at peak load the notch starts opening and the ultimate CMOD is two times the ultimate CMSD. This indicates that the fracture propagates in a combination of mode I and mode II with mode I prevailing.

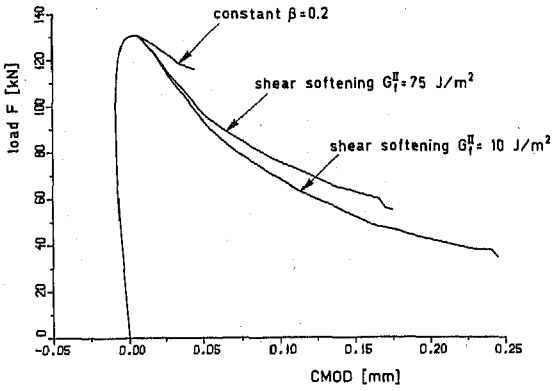


**FIG. 5. Load versus CMOD**

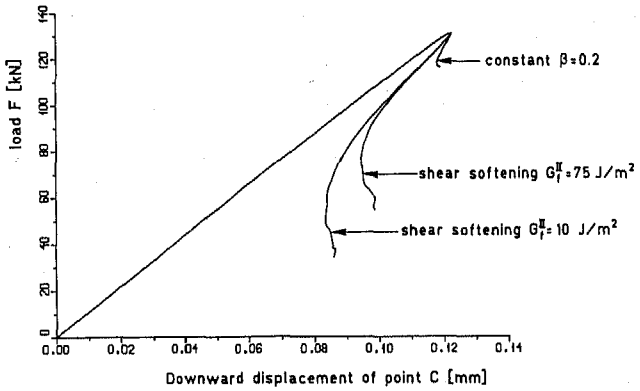


**FIG. 6. Load-Deflection Curves of Point C (see Fig. 3)**

If the steel beam of the test rig is assumed to be infinitely stiff, the vertical displacement of the point of load application C can be recalculated from the vertical displacements of points A and B (Fig. 3). This results in the load-deflection curves of Fig. 6, which exhibit a violent snap-back behavior. This snap-back explains why direct displacement control cannot produce a fully converged solution after peak load (De Borst 1986). Only with indirect CMSD control (or perhaps with CMOD control) and a full Newton-Raphson iterative procedure can a fully converged solution be obtained in the vicinity of the peak load. Unfortunately, the experimental load-deflection curves have not been reported by Arrea and Ingraffea (1982), so that a direct comparison with the experimental results is not possible.

Nevertheless, Figs. 4 to 6 show that the solution could not be continued until the load had dropped to zero. This is because at a certain stage in the post-peak regime two negative pivots were found upon factorizing the

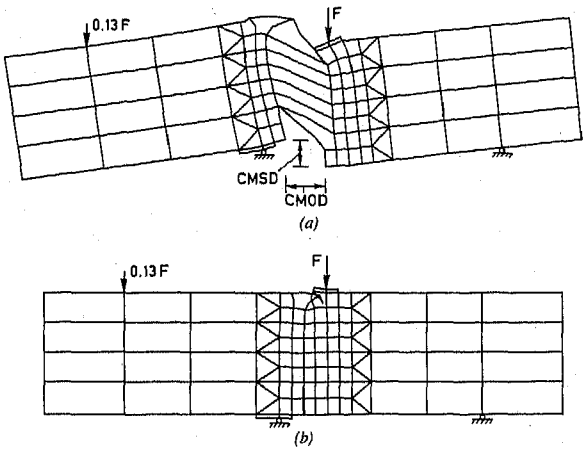


**FIG. 7. Eigen-Displacement Fields at Ultimate Residual Load**

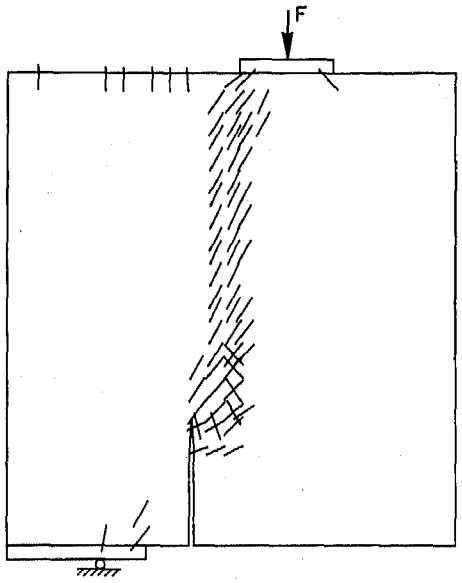


**FIG. 8. Crack Pattern at Ultimate Residual Load**

tangent stiffness matrix, whereafter a converged solution could no longer be obtained. An eigenvalue analysis was performed and for the analysis with $G_f^{II} = 75$ J/m$^2$ two negative eigenvalues (with the eigenmodes plotted in Fig. 7) resulted. One of the eigenmodes has a physical meaning as it represents the fracture localization that has developed over the entire depth of the beam. The other eigenmode is of a numerical nature because it represents a spurious hour-glass mode of only one element at the top of the beam.

Spurious hour-glass modes pose a serious problem because they may

easily cause divergence of the iterative procedure. Dodds et al. (1982) were probably the first to recognize the possibility of hour-glassing when performing finite element analyses of crack propagation. Based on their experiences using a simple crack model with a sudden stress drop upon fracture, they recommended to abandon the reduced four-point Gaussian quadrature and to employ nine-point Gaussian quadrature instead. However, later studies based on more advanced tensile softening models have indicated that the nine-point scheme may also give rise to hour-glass modes (de Borst 1986; Crisfield 1986; Rots 1985b). The present study confirms this, and the problems have been found to be even greater because of the allowance for multidirectional cracking and shear softening.

The low value for the mode II fracture energy $G_f^{II} = 10$ J/m$^2$ yields an even more pronounced structural softening than $G_f^{II} = 75$ J/m$^2$ (Figs. 4 to 6). However, the peak load does not seem to be markedly affected, which indicates that mode I effects prevail before peak. The same trend was observed upon an increase of $G_f^{II}$ (e.g., $G_f^{II} = 500$ J/m$^2$) and upon an increase of the ultimate crack shear stress $\tau_u$. Again, the peak load was not markedly affected and deviations were found only during the post-peak regime.

This section is concluded with the crack pattern of Fig. 8, which has been obtained for $G_f^{II} = 75$ J/m$^2$.

## Double-Notched Specimen

The second specimen, tested by Bažant and Pfeiffer (1986), bears similarities to the preceding one, but has a pair of symmetric notches instead of a single notch. Furthermore, the concentrated vertical loads were applied even closer to the notches, so as to produce an even narrower

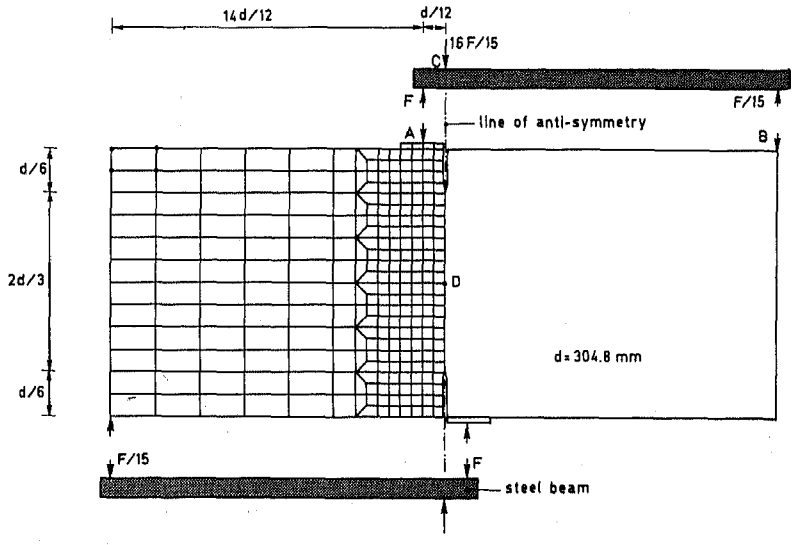


**FIG. 9. Finite Element Discretization for Double-Notched Specimen**

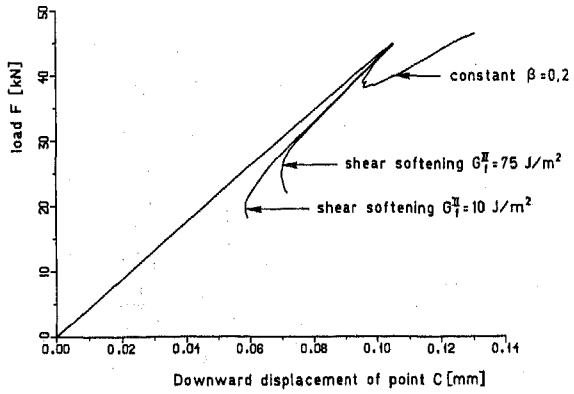


**FIG. 10. Load-Deflection Curves of Point C (see Fig. 10) for Three Different Crack Shear Representations**

region of high, mode II intensity. Fig. 9 shows the finite element idealization, which could be confined to one half of the beam because of antisymmetry. The antisymmetry was introduced by means of dependence relations. The beam had a thickness of 38.1 mm. In an attempt to avoid spurious hour-glass modes exhibited by the quadratic elements, we have resorted to linear four-noded elements with four-point Gaussian quadrature. Just as in the preceding analysis, the beam has been analyzed under CMSD control, and a full Newton-Raphson procedure has been adopted.

The concrete has again been modeled as linearly elastic in compression with a Young's modulus $E_c = 25{,}000$ N/mm$^2$ and a Poisson ratio $\nu = 0.2$. The mode I crack parameters have been taken as tensile strength $f_{ct} = 3$

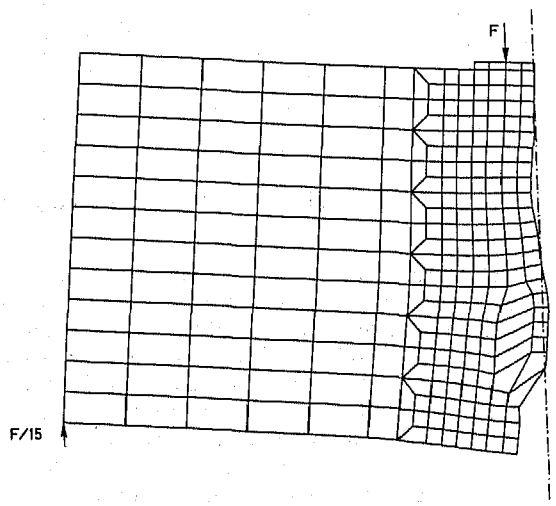


**FIG. 11. Eigen-Displacement Field at Peak Load**

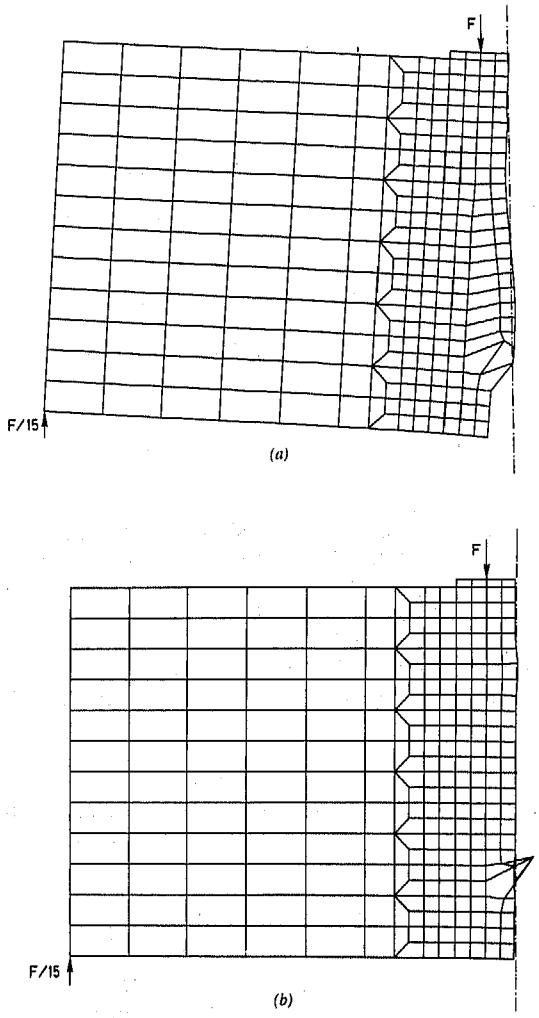


**FIG. 12. Eigen-Displacement Fields at Ultimate Residual Load**

N/mm$^2$; mode I fracture energy $G_f^I$ = 75 J/m$^2$; and intercrack threshold angle $\alpha$ = 60° (de Borst and Nauta 1985). The crack band width was estimated as $h$ = 12.7 mm. Again, three analyses are reported, one analysis corresponding to a constant shear retention factor $\beta_0$ = 0.2 ($D_0^{II}$ = 2,604 N/mm$^2$) and two analyses with shear softening with mode II fracture energy values of $G_f^{II}$ = 75 J/m$^2$ and $G_f^{II}$ = 10 J/m$^2$, respectively. For the latter two computations the ultimate shear stress was taken as $\tau_u$ = 0.5 N/mm$^2$ and the initial shear retention factor was taken as $\beta$ = 0.2.

Fig. 10 shows the computational results in terms of load-deflection curves for the loading point C of steel beam AB (Fig. 9). The deflection is defined as the difference between the vertical displacements of point C and of the center of antisymmetry, point D. The behavior is fairly similar to

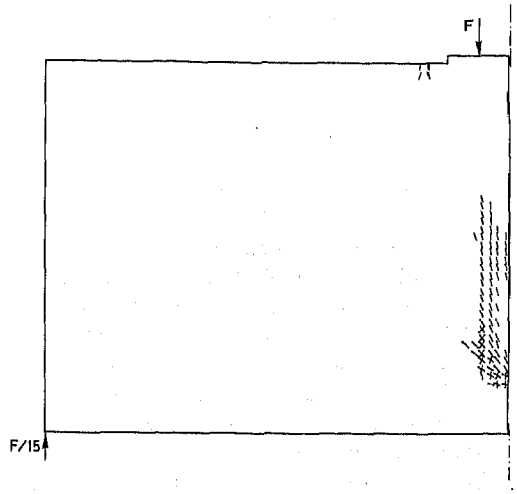


**FIG. 13. Crack Pattern at Ultimate Residual Load**

that of the preceding beam. Again, the constant shear retention factor yields too little softening. It even yields a spurious ascending branch in the post-peak regime, whereas the analyses including shear softening do not. The numerical prediction of the peak load appears to correspond well with the experimental value ($F = 44.8$ kN) and does not seem to be sensitive to the adopted representation for the shear transfer across the crack.

The finite element results for the analysis with $G_f^{II} = 75$ J/m$^2$ will now be considered in somewhat greater detail. At peak load an eigenvalue analysis of the tangent stiffness matrix was performed, which resulted in one negative eigenvalue with the eigenmode of Fig. 11, showing that the fracture localization has developed only partially at peak. After peak, the load was decremented and the solution could be continued up to the point where the load-deflection curve is terminated. Then, a second negative pivot was encountered upon factorizing the tangent stiffness matrix and a truly converged solution could no longer be obtained. An eigenvalue of the tangent stiffness matrix yielded two negative eigenvalues, with the eigenmodes plotted in Fig. 12. Similar to the analysis of the preceding beam, one eigenmode is of a physical nature and represents the fracture localization, which has continued propagating towards the opposite notch. The other eigenmode again represents a spurious hour-glass mode, which occurred because the group of elements surrounding a particular node was completely cracked. Obviously, the use of four-point integrated linear elements instead of nine-point integrated quadratic elements does not seem to eliminate the possibility of hour-glass mechanisms.

The eigenmodes in Figs. 11 and 12 reveal that the fracture discontinuities (there are two of them because of antisymmetry) first propagate slightly sideways from the notches and then continue to propagate in the vertical direction towards the opposite notch. This observation is in line with the crack pattern of Fig. 13. The crack pattern exhibits quite a number of multiply cracked sampling points, which indicates that stress rotations

after primary cracking have been significant, even though shear softening has been added.

## Does Mode II Concrete Fracture Exist?

A lively discussion currently centers around the issue of whether mode II (shear) fracture in concrete exists or not. Based on their experiences with the single-notched specimen geometry of Fig. 3, Arrea and Ingraffea (1982) and Ingraffea and Gerstle (1985) conclude that concrete fractures in mode I even if a high, mode II intensity is present. More recently, Ingraffea and Panthaki (1985) have sharpened this conclusion by presenting finite element results for the double-notched shear beam tested by Bažant and Pfeiffer (Fig. 9), which reveal that this specimen must have failed in mode I also. This contrasts with the observations by Bažant and Pfeiffer (1986), who state that "failure is due essentially to shear fracture (mode II)".

It is striking that our results for the single-notched beam of Arrea and Ingraffea (1982) and the double-notched beam of Bažant and Pfeiffer (1986) exhibit a fairly similar fracture localization pattern. In both cases the cracks first propagate slightly curvilinearly and then continue to propagate in a vertical direction. Furthermore, close examination of the finite element outputs revealed that the mode I fracture energy was released much quicker than the mode II fracture energy in both cases, which suggests that fracture predominantly propagates in mode I.

Nevertheless, a pure mode I fracture has not occurred. This, of course, only happens if mode II displacements are suppressed completely, i.e., if a constant shear retention factor $\beta = 1$ is adopted. For the beam of Bazant and Pfeiffer (1986), such an additional analysis has been undertaken, and it resulted in the fracture localization shown in Figs. 14 and 15. The curvilinear cracks are more pronounced and isolated cracking occurs in the middle of the specimen because of the existence of horizontal tensile stresses, as was demonstrated before by Rots (1985a). This behavior closely resembles the prediction by Ingraffea and Panthaki (1985) and bears similarities with the failure mode in the Brazilian split cylinder test. Since the present study indicates that the use of a constant shear retention factor should be rejected, especially when it is equal to 1, a pure mode I mechanism is not believed to represent the fracture mechanism that has occurred in the tests.

More information regarding the question above might be obtained by considering the energy balance. Ignoring energy dissipation by mechanisms other than fracture, the energy supplied to a specimen, which is represented by the integral load(s) versus displacement(s) at the loading point(s), should balance the fracture energy times the area which has fractured. In the mixed-mode experiments of Arrea and Ingraffea (1982) and Bažant and Pfeiffer (1986), the final fracture surface has been recorded, but the overall load-displacement curves have not been published. Consequently, a mode I, mode II or combined mixed-mode fracture energy value, which is needed in case of strain-softening finite element predictions, cannot be directly extracted from the experimental results.

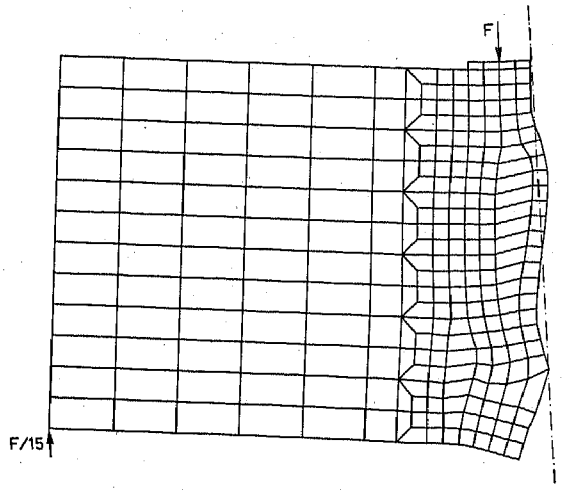


**FIG. 14. Fracture Localization for $\beta = 1$**

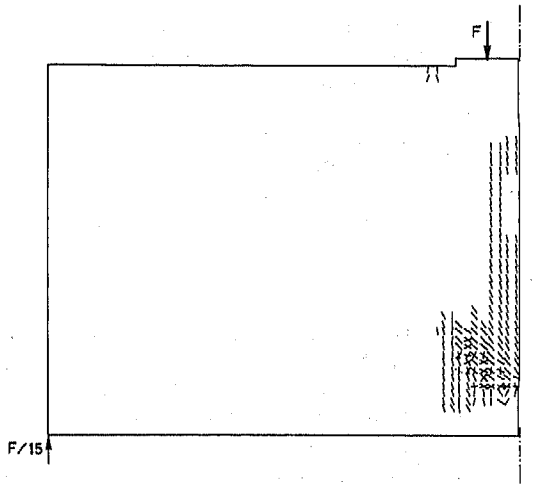


**FIG. 15. Crack Pattern for $\beta = 1$**

## CONCLUSIONS

A shear softening formulation was incorporated in a recently proposed smeared crack model (de Borst and Nauta 1984, 1985; Rots et al. 1985). In this paper a simple bilinear relation was adopted for the shear softening model, but the framework of the crack model permits implementation of a wide variety of formulations.

The present shear softening formulation has been set up along lines similar to those of the tensile softening model by Bažant and Oh (1983). It

involves a maximum shear stress $\tau_u$, which can be transferred, and a fracture energy $G_f^{II}$, which can be dissipated in mode II crack propagation, as material parameters and a definition of the shape of the shear softening curve.

The present shear softening formulation has been applied to two notched, unreinforced beams. Comparison with experimental data clearly demonstrates that the results of the computations including shear softening are superior to the results obtained with a conventional constant sheer retention factor, since the computations with a constant shear retention factor showed much too little structural softening in the post-peak regime.

The computational results further show that snap-back behavior may occur under quasistatic loading conditions when softening stress-strain laws are employed. This observation has been made before by Crisfield (1986) and by de Borst (1986) for tension softening models, but holds even stronger when a shear softening model is included in the analysis.

A serious problem that may arise during calculations with softening models is the occurrence of hour-glass modes. This was noticed first by Dodds et al. (1982), who demonstrated that four-point Gaussian integration is not suitable for smeared crack analysis with eight-noded elements. The present study indicates also that the eight-noded element with a nine-point integration scheme and the four-noded bilinear element with four-point integration are not free from this phenomenon. It has been demonstrated that these hour-glass mechanisms may even dominate the response in the post-peak regime, especially when shear softening is added or when we permit multiple crack formation.

The present study does not reveal the existence of pure mode II fracture in concrete; neither does it support the assertion that concrete always fractures in mode I. It rather shows a mixed-mode mechanism with tensile softening effects prevailing before peak and shear softening effects gradually become more important in the post-peak regime.

## Acknowledgments

The calculations reported in this paper were performed with the DIANA (a trademark of TNO Institute for Building Materials and Structures) finite element code on the VAX 11/780 and the SEL/GOULD computer facilities of TNO-IBBC. Support from the DIANA group is gratefully acknowledged. Parts of the research reported in this paper were assisted financially by CUR-Committee A 26, "Concrete Mechanics," and by the Netherlands Technology Foundation (STW). The first writer's contribution is part of a STW research project under the supervision of J. Blaauwendraad of Delft University of Technology.

## Appendix. References

Arrea, M., and Ingraffea, A. R. (1982). "Mixed-mode crack propagation in mortar and concrete." *Report No. 81-13*. Dept. of Struct. Engrg., Cornell Univ., Ithaca, N.Y., 143 pp.

Bažant, Z. P., and Gambarova, P. (1980). "Rough cracks in reinforced concrete." *J. Struct. Div.*, ASCE, 106(4), 819–842.

Bažant, Z. P., and Oh, B. H. (1983). "Crack band theory for fracture of concrete." *Materiaux et Constructions* (RILEM) 16, 155–177.

Bažant, Z. P., and Pfeiffer, P. A. (1986). "Shear fracture tests of concrete." *Materiaux et Constructions* (RILEM) 19, 111–121.
de Borst, R., and Nauta, P. (1984). "Smeared crack analysis of reinforced concrete beams and slabs failing in shear." *Proc. Int. Conf. on Computer Aided Analysis and Design of Concrete Struct.*, F. Damjanić et al., eds., Part 1, Pineridge Press, Swansea, 261–273.
de Borst, R., and Nauta, P. (1985). "Non-orthogonal cracks in a smeared finite element model." *Engrg. Computations* 2, 35–46.
de Borst, R. (1986). "Non-linear analysis of frictional materials." *Dissertation*, presented to Delft University of Technology, at Delft, Netherlands, in partial fulfillment of the requirements for the degree of Doctor of Philosophy.
de Borst, R., and van den Berg, P. (1986). "Analysis of creep and cracking in concrete members." *Preprints, 4th RILEM Symp. on Creep and Shrinkage of Concrete: Mathematical Modeling*, Z. P. Bažant, ed., Northwestern Univ., Evanston, Ill.
Cedolin, L., and Dei Poli, S. (1977). "Finite element studies of shear-critical R/C beams." *J. Engrg. Mech. Div.*, ASCE, 103(3), 395–410.
Cornelissen, H. A. W., Hordijk, D. A., and Reinhardt, H. W. (1986). "Experimental determination of crack softening characteristic of normal weight and lightweight concrete." *HERON* 31(2), 45–56.
Crisfield, M. A. (1981). "A fast incremental/iterative procedure that handles snapthrough." *Computers and Struct.* 13, 55–62.
Crisfield, M. A. (1986). "Snap-through and snap-back response in concrete structures and the dangers of under-integration." *Int. J. for Numerical Methods in Engrg.* 22(3), 751–768.
Dodds, R. H., Darwin, D., Smith, J. L., and Leibengood, L. D. (1982). "Grid size effects with smeared cracking in finite element analysis of reinforced concrete." *SM Report No. 6*. Univ. of Kansas, Lawrence, Kans., 118 pp.
Glemberg, R. (1984). "Dynamic analysis of concrete structures." *Publication 84:1*. Dept. of Struct. Mech., Chalmers Inst. of Tech., Göteborg, 134 pp.
Hillerborg, A., Modeer, M., and Petersson, P. E. (1976). "Analysis of crack formation and crack growth in concrete by means of fracture mechanics and finite elements." *Cement and Concrete Res.* 6 (6), 773–782.
Ingraffea, A. R., and Gerstle, W. (1985). "Nonlinear fracture models for discrete crack propagation." *Application of fracture mechanics to cementitious composites*, S. P. Shah, ed., Martinus Nijhoff Publishers, Dordrecht, 247–285.
Ingraffea, A. R., and Panthaki, M. J. (1985). "Analysis of 'shear fracture' tests of concrete beams." *Preprints, US-Japan Seminar on Finite Element Analysis of Reinforced Concrete Struct.* 1, Tokyo, 71–91.
Kolmar, W., and Mehlhorn, G. (1984). "Comparison of shear stiffness formulations for cracked reinforced concrete elements." *Proc. Int. Conf. on Computer Aided Analysis and Design of Concrete Struct.*, F. Damjanić et al., eds., Part 1, Pineridge Press, Swansea, 133–147.
Leibengood, L., Darwin, D., and Dodds, R. H. (1986). "Parameters affecting FE analysis of concrete structures." *J. Struct. Engrg.*, ASCE, 112(2), 326–341.
Litton, R. W. (1974). "A contribution to the analysis of concrete structures under cyclic loading." *Dissertation* presented to the University of California, at Berkeley, Calif., in partial fulfillment of the requirements for the degree of Doctor of Philosophy.
Ramm, E. (1981). "Strategies for tracing the nonlinear response near limit points." *Nonlinear Finite Element Analysis in Structural Mechanics*. Springer Verlag, Berlin, Germany, 63–83.
Reinhardt, H. W., and Walraven, J. C. (1982). "Cracks in concrete subject to shear." *J. Struct. Div.*, ASCE, 108(1), 207–224.
Riggs, H. R., and Powell, G. H. (1986). "Rough crack model for analysis of concrete." *J. Engrg. Mech.*, ASCE, 112(5), 448–464.
Riks, E. (1979). "An incremental approach to the solution of snapping and buckling problems." *Int. J. Solids and Struct.* 15, 529–551.
Rots, J. G., Kusters, G. M. A., and Blaauwendraad, J. (1984). "The need for

fracture mechanics options in finite element models for concrete structures." *Proc. Int. Conf. on Computer Aided Analysis and Design of Concrete Struct.*, F. Damjanić et al., eds., Part 1, Pineridge Press, Swansea, 19–32.
Rots, J. G., Nauta, P., Kusters, G. M. A., and Blaauwendraad, J. (1985). "Smeared crack approach and fracture localization in concrete." *HERON* 30(1) 48 pp.
Rots, J. G. (1985a). "Strain-softening analysis of concrete fracture specimens." *Fracture toughness and fracture energy of concrete*, F. H. Wittmann, ed., Elsevier Science, Amsterdam, Netherlands, 137–148.
Rots, J. G. (1985b). "Bond-slip simulations using smeared cracks and/or interface elements." *Res. Report.* Struct. Mech. Group, Dept. of Civ. Engrg., Delft Univ. of Tech., 56 pp.
Suidan, M., and Schnobrich, W. C. (1973). "Finite element analysis of reinforced concrete." *J. Struct. Div.*, ASCE, 99(10), 2109–2122.
Willam, K. J., and Sture, S. (1985). "A composite fracture model for localized cracking cementitious materials." *Proc. 2nd Symp. on Interaction of Non-Nuclear Munitions with Struct.*, P. Y. Thompson et al., eds., Univ. of Florida, Panama City Beach, Florida.